Magnetotransport properties of nearly-free electrons in two-dimensional hexagonal metals and application to the $M_{n+1}AX_n$ phases

T. Ouisse,[1,*] L. Shi,[1,2] B. A. Piot,[3] B. Hackens,[2] V. Mauchamp,[4] and D. Chaussende[1]

[1]*Laboratoire des Matériaux et du Génie Physique (LMGP), Unité Mixte de Recherche (UMR) du Centre National de la Recherche Scientifique (CNRS) 5628, Institut National Polytechnique de Grenoble (INPG), Minatec, 3, parvis Louis Néel, 38016 Grenoble, France*

[2]*Institut de la Matière Condensée et des Nanosciences, NAnoscopic PhySics (IMCN/NAPS), Université Catholique de Louvain, 2 Chemin du Cyclotron, 1348 Louvain-la-Neuve, Belgium*

[3]*Laboratoire National des Champ Magnétiques Intenses (LNCMI), Centre National de la Recherche Scientifique (CNRS), Université Joseph Fourier (UJF), Institut National des Sciences Appliquées (INSA), European Magnetic Field Laboratory (EMFL), 25, rue des Martyrs, 38042, Grenoble, France*

[4]*Institut Pprime, Unité Propre de Recherche (UPR) 3346 du Centre National de la Recherche Scientifique (CNRS), Université de Poitiers, Institut Supérieur de l'Aéronautique et de l'Espace (ISAE), Ecole Nationale Supérieure de Mécanique et d'Aérotechnique (ENSMA), Sciences, Physique, Mécanique, Mathématiques et Informatique (SP2MI) Téléport 2, BP 30179, 86962 Futuroscope-Chasseneuil Cedex, France*

(Received 28 April 2015; revised manuscript received 3 July 2015; published 31 July 2015)

We propose a general, yet simple model for describing the weak field magnetotransport properties of nearly-free electrons in two-dimensional hexagonal metals. We modify this model so as to apply it to the magnetotransport properties of the $M_{n+1}AX_n$ phases, a particular class of nanolamellar carbides and nitrides. We argue that the values of the in-plane Hall coefficient and the in-plane parabolic magnetoresistance are due to the specific shape of the Fermi surface of almost two-dimensional hole and electron bands. If the contribution of the electron pockets to in-plane resistivity is often (but not always) predicted to be a minor one, in contrast, both holes and electrons should substantially contribute to the overall value of the in-plane Hall coefficient. The relevance of our model is supported by elementary considerations and a set of experimental data obtained from single crystals of V_2AlC and Cr_2AlC. In particular, we obtain a high ratio between the in-plane (ρ_{ab}) and parallel to the c axis (ρ_c) resistivities.

DOI: 10.1103/PhysRevB.92.045133 PACS number(s): 72.15.Eb, 72.15.Gd, 72.15.Lh

I. INTRODUCTION

Explaining transport in metals is often a complex matter, because transport coefficients are mainly determined by the local curvature of the Fermi surface [1–3], and the Fermi surface of even the most common metallic elements may indeed reveal a very complex and intricate shape, with the presence of both electrons and holes [1–3]. Isotropic effective mass models usually work well for describing the gross features of electron transport in semiconductors because all the relevant physics occurs near the top or the bottom of the valence and conduction band, respectively, so that the dispersion law is parabolic. Even if the effective mass is anisotropic, transport phenomena do not qualitatively change, but the fact is that this anisotropy may give rise to a magnetoresistance. In contrast, the relevance of such models to metals is highly uncommon because the Fermi level E_F is located much deeper inside the bands, so that the Fermi surface often exhibits a very complex shape. In metals, the transport coefficients essentially depend on this shape and on the relaxation time values, the latter depending partly on the former [1–4]. Most often, the dependence of the resistivity ρ with temperature T primarily reflects the variation of the relaxation time with T, whereas the carrier density does not appreciably vary [3], yet the Hall coefficient R_H may change with T [5] or, even stranger, may reverse its sign when sweeping either T or the magnetic field $\mathbf{B}$ [2].

Among the family of compensated metals, $M_{n+1}AX_n$ (or "MAX") phases form an interesting class of hexagonal carbides and nitrides (M is a transition metal, A belongs to groups 13–16, and X is the C or N element) [6]. In their single-crystalline form, they possess a highly anisotropic nanolamellar structure [6,7]. They can be viewed as a stack of hexagonal planes, each plane including only one kind of chemical element. They combine interesting properties of ceramics to that of metals [6,7]. They are expected to play a major role in applications requiring high chemical stability, high temperature, shock resistance, and good electrical conductivity [6,7]. These phases can also behave as self-healing materials [8]. Additionally, the planes of the weakly bonded A atoms can be chemically removed in order to form a new class of two-dimensional (2D) systems called MXenes [9]. Some recently engineered MAX phases also exhibit potentially attractive magnetic properties [10].

So far, most of the produced samples were highly polycrystalline, so that it was not possible to evidence anisotropic physical properties in a straightforward manner. In recent years, several groups have produced single crystals of MAX phases in the form of bulk crystals [11–13] or thin layers [14–17]. It thus becomes feasible to investigate anisotropic physical properties such as electrical transport [16]. In polycrystalline phases, Hall data indicate that these materials behave as compensated metals (or semimetals). They exhibit a small R_H and an almost parabolic positive magnetoresistance [18–22]. Interpretation of the data is usually made by assuming the existence of two isotropic bands of electrons and holes with similar densities ([6], and references therein). In this paper, we will refer to this model as the isotropic or "conventional" two-band model. Further data extraction then shows that both carrier mobilities should also be quite similar [6]. This would

*thierry.ouisse@phelma.grenoble-inp.fr

tend to indicate that electrons and holes exhibit very similar properties, a point yet to be explained in the literature about MAX phases [6]. A review of electrical transport data in those phases can be found in chapter 5 of [6]. Recently, and based on density functional theory (DFT) calculations, some authors have argued that, for Ti_2AlC, hole transport should prevail in the basal plane, whereas electron transport would dominate along the c axis [16]. Electrons and hole properties would thus be very different, in contrast with the interpretation given by the conventional two-band model. Additionally, we note that, if transport is highly anisotropic in single crystals, data obtained from isotropic polycrystalline phases depend in a complex manner on the grain size and orientation, grain boundaries, texture, etc., so that it is difficult to draw firm general conclusions about single crystals from data obtained from polycrystals and reciprocally.

The first purpose of this paper is to derive a simple though hypothetical model, based on general properties of nearly-free electrons (NFEs) in 2D hexagonal metals. A nice introduction to the physical phenomena which determine magnetotransport properties in 2D metals can be found in Ong's paper [1]. In Sec. II, we apply some of the principles presented in [1] to the case of a hexagonal symmetry. This model is subsequently modified so as to adapt it to the description of in-plane transport in the MAX phases. It would be naïve to think that the NFE approach can capture the physics of all MAX phases, but we show that it can be used to mimic the Fermi surface of some of them convincingly and to point out the two essential features which govern transport: the local Fermi velocity $\mathbf{v}_F$ and the local curvature of the Fermi surface. None of those quantities are simply related to the real electron and hole densities. This analysis forms the first part of this article (Sec. II). Our second goal is to provide both in-plane and c axis transport data measured from single crystals. The latter are grown in a high temperature metallic solution and processed so as to form Hall bars, Van der Pauw samples, and devices aimed at measuring ρ_c when the crystal aspect ratio is not favorable. Interestingly, combining basic results about the Fermi surface of a 2D hexagonal metal to simple geometric considerations and to reasonable orders of magnitude for physical quantities, such as the relaxation time and the number of valence electrons, allows us to recover many experimental facts, at least in the case of the two investigated phases (Cr_2AlC and V_2AlC). This forms the second part of our report (Sec. III). Eventually, we summarize our results. We also discuss the relevance of using isotropic one- or two-band models and address open problems.

II. THEORY

A. Adaptation of the NFE model to the MAX phases

As emphasized by Ashcroft and Mermin in 1976, the free-electronlike Fermi surfaces are essential in understanding the real Fermi surfaces of many metals [3]. We intend to argue that at least some MAX phases probably make no exception. Determining the Fermi line of NFEs in a pure 2D hexagonal metal is elementary. It involves only one energy term U, the Fourier component of the periodic potential for a wave vector joining the centers of two adjacent Brillouin zones (BZs). By following a procedure exposed, e.g., in Ref. [3], and for a high

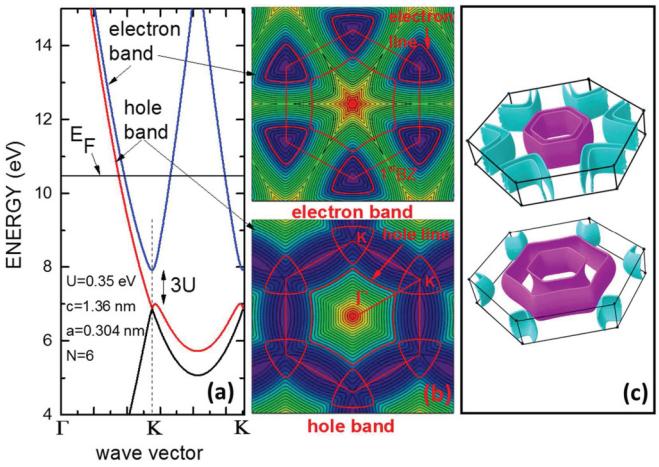

FIG. 1. (Color online) (a) Dispersion curves of NFEs in a 2D hexagonal lattice (b) contour plot of the energy (the red lines are the Fermi lines of the hole and electron bands), and (c) Fermi surfaces obtained by combining an in-plane, 2D NFE dispersion, and a tight-binding coupling between the transition metal planes (in the lower figure, the interplane-induced splitting and N are such that only the electron pockets with a lower energy are populated). Different splitting are assumed for the holes and electrons.

enough number of electrons per unit cell, we obtain electron pockets and a hole band centered at the origin [Figs. 1(a) and 1(b)]. We define N as the number of electrons per unit cell populating all partially filled bands, and in order to compare the model to the case of the M_2AX phases, or to compute three-dimensional (3D) carrier densities from the 2D model, we assume that we have four 2D planes per unit cell (one must thus divide N by a factor of 4 to get the number of electrons per plane in partially filled bands). There is already a striking similarity between the Fermi line of the 2D model [Fig. 1(b)] and the computed 3D Fermi surface of Ti_2AlC [Fig. 2(b); calculation details are given in Appendix A]. However, a major difference lies in the splitting of the hole band appearing in Fig. 2(b). Direct inspection of the atomic lattice [Fig. 2(a)]

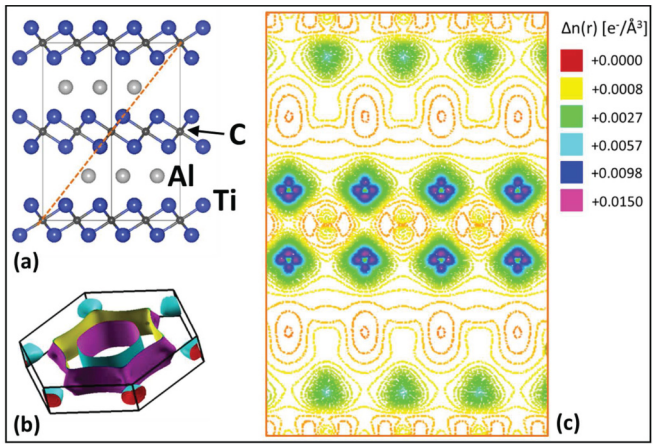

FIG. 2. (Color online) (a) Atomic structure of Ti_2AlC in real space. The dotted line corresponds to a TiC plane. (b) Fermi surface as computed by DFT calculations and (c) contour plot of the density of electrons around the Fermi level in a TiC plane, as computed by DFT calculations.

shows that, for a M_2AX phase, the M planes form close pairs separated by an X plane, which are in turn separated from one another by the more distant A planes. Figure 2(c) shows the density of electrons lying in the partially occupied bands as a function of the position in a "TiC" plane [defined by the dotted line in Fig. 2(a)]. It shows that, in real space, the electrons at E_F are confined in the M planes, as confirmed by the many reported density of states calculations, which all evidence that the M states dominate at E_F (see [16] and [23] among others). If we first neglect the different zigzag orientations between two adjacent A planes, we can form a reduced lattice with two inequivalent M planes per reduced unit cell, which are responsible for the large band splitting. Then in the spirit of what is often achieved for the quasi-2D cuprates, we treat independently the electrons as nearly free in the M planes and as strongly confined along **c**. This allows us to apply a simple tight-binding approach to the wave vector component along **c**, resulting in a **c** axis dispersion and splitting of the form $E = E_0 \pm (\beta^2 + \gamma^2 + 2\beta\gamma\cos(k_z c))^{1/2}$, where E_0, β, and γ are energy terms fixed by the lattice properties (we roughly assume that interplane coupling does not preferentially occur at given atom lattice sites). Summing the in-plane and out-of-plane energy contributions gives rise to Fermi surfaces as in Fig. 1(c). The similarity with DFT calculations [Fig. 2(b)] is striking, even if so simple a model can obviously not reproduce the smallest details. In particular, this approach neglects an additional but quite small splitting, which dissociates each hole surface into almost undistinguishable surfaces. This can be attributed to the fact that two consecutive M_2X planes are inequivalent [see Fig. 2(a)]. The DFT calculations also indicate that only the lowest split electron pockets are occupied, whereas each of the split hole bands are occupied (there are thus four occupied hole bands and just one set of occupied electron pockets). This is not predicted by our simplified model.

In order to further simplify the calculation of all transport parameters, we move one last step further and replace the 3D structure by a fully 2D model, neglecting any energy variation along c (so that we can only predict the values of in-plane transport coefficients). This gives Fermi lines such as the one presented in Fig. 3. It is obtained by using the right number of electrons per unit cell lying in partially filled bands for Ti_2AlC, $N = 6$. Comparing it to the projection of a full numerical computation in the basal plane demonstrates that only the small features are not reproduced, as well as the lack of degeneracy of the electron pockets with respect to that of the holes (Fig. 3). In the case of Ti_2AlC, the roughest approximation is to consider that the electron pockets form open tubes, which is actually not predicted by DFT calculations [see Fig. 2(b)], and we also have to reduce the valley degeneracy of the electron pockets g_n by a factor of 2 with respect to that of the hole bands. The former point means that the simplified model probably slightly overestimates the contribution of electrons to in-plane transport. Such a point can be empirically improved by finding a set of energy parameters which slightly underestimates the extent of those electron pockets (as achieved in Fig. 3).

Compiling the published expectations for other MAX phases shows that the overall structure of the Fermi surface is most often formed by hexagonally shaped hole bands in the center of the zone and by trigonal electron pockets extending over three hexagonal BZs and centered at the corners of the

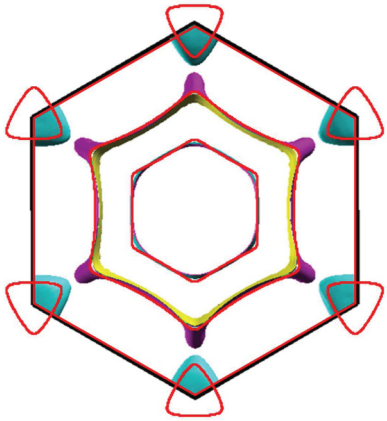

FIG. 3. (Color online) Projection in the basal plane of the Ti_2AlC Fermi surface obtained from the DFT calculations (all colors but red), along with the fit of the Fermi line given by the 2D model using $U = 0.35$ eV, $N = 6$, and an appropriate interplane-induced splitting (red lines).

BZ hexagon [16,23,24]. Some of the electron pockets often form open tubes too. The number of bulges appearing in the open tubes over one unit cell is a direct function of the integer n appearing in the $M_{n+1}AX_n$ formula. In one case (Ti_3AlC_2), the "electron" bands are repelled at energies high enough for being totally unoccupied [24]. Although not so many Fermi surface calculations are available in the literature, most of them roughly support the NFE origin of the Fermi surface shape. Our purpose is therefore to use the 2D model as a reasonable approximation of the Fermi surface shape (which works at least for Ti_2AlC) because it allows us to simplify the calculation of the transport parameters considerably and to focus on physical aspects. Of course, this approximation is totally unable to reproduce the fine structure of the electron pockets which is sometimes found by DFT calculations (see, e.g., [16,22–24]), and it restricts the analysis to in-plane transport, but accurate results would not only require an exact knowledge of the Fermi surface. They demand a precise knowledge of the dependence of the scattering times τ_n (electrons) and τ_p (holes) upon wave vector $\mathbf{k}_F$ and temperature, a thing which is simply impossible to obtain experimentally. Our model allows us to vary τ_n and τ_p independently and therefore to assess whether a modification of their ratio may have observable consequences. We can also compute the magnetoresistance. Those two possibilities are not available from the commercial numerical codes used by previous authors [16,22–24]. Therefore, our simplified model is aimed at finding correct orders of magnitude on a physical basis and at identifying the essential parameters governing transport. When the Fermi surface is complex, isotropic transport models do not rely on a realistic basis, yet they are the only ones which can easily be used for data extraction (e.g., for giving carrier densities and mobilities). We aim at discussing if these extracted parameters can bear any resemblance to the real physical values.

B. Transport formalism

Here, we briefly summarize the principle used for calculating the transport coefficients. As usual, we start from

Boltzmann's equation, where **F** is the force, including the electrical and Lorentz contributions, f_0 is the equilibrium distribution, and τ is the relaxation time

$$\frac{\mathbf{F}}{\hbar}\nabla_{\mathbf{k}}(f_0+\Delta f)+\frac{\Delta f}{\tau}=0. \tag{1}$$

From this equation, the out-of-equilibrium part Δf of the distribution function is expressed as

$$\Delta f=-\left[1+\frac{e\tau}{\hbar}(\mathbf{v}\times\mathbf{B})\frac{\partial}{\partial\mathbf{k}}\right]^{-1}e\tau\,\mathbf{v}.\boldsymbol{\varepsilon}\,\frac{\partial f}{\partial E}, \tag{2}$$

where **v** is the velocity, **B** the magnetic field, and $\boldsymbol{\varepsilon}$ the electric field. If **B** is parallel to **c** (itself parallel to z) and $\boldsymbol{\varepsilon}$ is parallel to x, expanding the denominator gives (Jones-Zener approximation) [25]

$$\Delta f=-\left[1-\frac{e\tau}{\hbar}\left(B\mathrm{v}_y\frac{\partial}{\partial k_x}-B\mathrm{v}_x\frac{\partial}{\partial k_y}\right)+\text{ order 2}\right]\times e\tau\,\mathbf{v}.\boldsymbol{\varepsilon}\frac{\partial f}{\partial E}. \tag{3}$$

The first term inside the parentheses gives rise to the direct conductivity σ_{XX} (without the magnetoresistance contribution), the second term (first order in B) gives rise to the transverse conductivity σ_{XY}, and the third term (second-order term in B) is at the origin of the magnetoresistance [here, we do not write its lengthy expression, but it is trivial to obtain it from Eq. (2)]. Here, Δf is used to compute any current component through

$$\mathbf{j}=\frac{e}{2\pi^2}\int\mathbf{v}(\mathbf{k})\Delta f d^2\mathbf{k}. \tag{4}$$

Computing j_x gives σ_{XX} and the magneto-resistance, and j_y leads to R_H. Additionally, a considerable simplification is obtained for a 2D system, since any transport integral can then be put into the form of a circulation along the Fermi line. Grouping all terms appearing in Eq. (3) except $\partial f/\partial E$ under the form of a function $g(\mathbf{k})$, any transport integral can be put in the polar form

$$\int g(k_x,k_y)\frac{\partial f}{\partial E}dk_xdk_y\cong\int g(\mathbf{k}_F)\frac{d\mathbf{k}_F}{\hbar v_F}=\int g(\mathbf{k}_F)\frac{1}{\hbar v_F}\sqrt{k_F^2+\left(\frac{\partial k_F}{\partial\theta}\right)^2}d\theta. \tag{5}$$

Roughly speaking, this means that, for interpreting magnetotransport, we just have to examine what the holes and electrons do along the Fermi line as a function of time (including scattering). From the calculations of the direct conductivities σ^i_{XX} and transverse conductivities σ^i_{XY} for each band of index i, one can obtain the overall resistivity and Hall coefficient values from summations of the kind

$$\rho_{ab}=\frac{\sum_i\sigma^i_{XX}}{\left(\sum_i\sigma^i_{XX}\right)^2+\left(\sum_i\sigma^i_{XY}\right)^2},\qquad R_H=\frac{\sum_i\sigma^i_{XY}}{\left(\sum_i\sigma^i_{XX}\right)^2+\left(\sum_i\sigma^i_{XY}\right)^2}\frac{1}{B}. \tag{6}$$

C. Predicted results for a simple 2D hexagonal metal

In this section, we use the simplest model, not directly mimicking the MAX phase Fermi surface, so as to emphasize and isolate various physical phenomena. The lattice parameters are nevertheless that of Ti_2AlC. As a first example, we select just a few electrons per unit cell, so that we only have holes as free carriers (Fig. 4.1), yet the calculations give a substantial magnetoresistance [Fig. 4.1(d)], and R_H is quite small, $R_H=1.178\times10^{-11}\,\mathrm{m^3C^{-1}}$. An isotropic one-band model would lead to an apparent hole density $p_{\mathrm{app}}=1/eR_H=5.30\times10^{29}\times\mathrm{m}^{-3}$, extremely far from the assumed value, $p=2.30\times10^{28}\,\mathrm{m}^{-3}$. To interpret these results, we first remember that, in a semiclassical approximation, the wave vector changes with time according to $\hbar\partial\mathbf{k}/\partial t=e\mathbf{v}\times\mathbf{B}$ due to the Lorentz force, so that holes with an energy E_F cycle clockwise along the Fermi line, until they are scattered to another part of it by a collision. If we focus on the concave part, and in contrast to this clockwise rotation, the hole velocity, which is perpendicular to the Fermi line, rotates counterclockwise with time [see Fig. 4.1(a)]. In real space, the holes are thus turning anticlockwise, so that during a fraction of time in between two collisions, they truly exhibit an electronlike behavior. It is only at the corners with a convex shape that their velocity rotates clockwise with time, so that they turn clockwise, as free holes would do in real space [Fig. 4.1(a)]. This phenomenon is discussed, e.g., in [1–2]. It dramatically affects the value of R_H. The holes behaving part of the time as electrons, and another part as holes, this leads to an apparent compensation and a smaller R_H value. Ong's theorem for 2D metals provides an elegant way to describe this [1]. It states that σ_{XY} is given by

$$\sigma^{2D}_{XY}=\frac{2e^3}{h^2}A_lB, \tag{7}$$

where A_l is the algebraic (i.e. oriented) area spanned by the mean free path as the wave vector cycles over one full orbit of the Fermi line. If the mean free path $\lambda=v_{\mathbf{k}}\tau_{\mathbf{k}}$ is a constant (e.g. for pure impurity scattering), one obtains a circle whose sign corresponds to the right type of carriers [1], but λ may vary with $\mathbf{k}_F$ [for instance, if the relaxation time $\tau_{\mathbf{k}}$ is isotropic and $\mathbf{v}_F$ is not constant along the Fermi line, see Figs. 4.1(b) and 4.2(b)]. For holes, the oriented area now exhibits outer flaps affected by a negative sign [see Fig. 4.1(c)], corresponding to the electronlike parts of the Fermi line. They must be subtracted from the holelike contribution [central part in Fig. 4.1(c)]. If the flaps get bigger than the central part, R_H can even reverse its sign [1]. For similar reasons (holes partially behaving as electrons and leading to seemingly compensated transport), holes alone can give rise to a magnetoresistance [1]. This is the case of our hexagonal 2D model [see Fig. 4.1(d)]. Using an extraction procedure assuming the existence of two kinds of carriers and $n=p$, as described in Appendix B, the parameters of Fig. 4.1 would lead to almost equal mobilities (96.2 and 93.5 $\mathrm{cm^2/V.s}$, respectively) and concentrations $n_{\mathrm{app}}=p_{\mathrm{app}}=7.36\times10^{27}\,\mathrm{m}^{-3}$. Here, we draw an intermediate conclusion (which is not original, see, e.g., Refs. [1,2]): Finding a small R_H value and a substantial magnetoresistance does not prove that two kinds of carriers are at play. Figure 4.1 even shows that a system involving just holes can mimic compensated transport

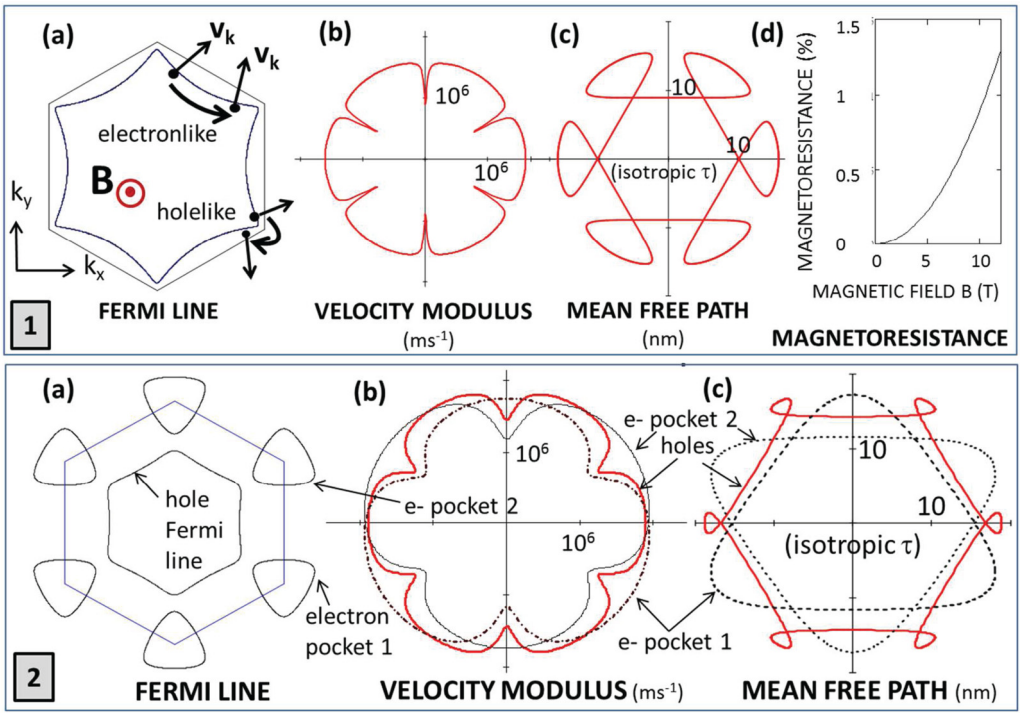

FIG. 4. (Color online) (1) (a) Fermi line, (b) polar plot of the velocity along the Fermi line, (c) polar plot of the mean free path, and (d) magnetoresistance of a 2D hexagonal system of NFEs with $N = 2$ ($\tau_p = 10^{-14}$ s, $U = 0.25$ eV, four 2D planes per unit cell, $c = 1.36$ nm and $a = 0.304$ nm). (2) (a) Fermi line, (b) radial plot of the velocity, and (c) mean free path for $N = 6$ ($\tau_p = \tau_n = 10^{-14}$ s, $U = 0.75$ eV, $c = 1.36$ nm and $a = 0.304$ nm).

with almost perfectly balanced electron and hole properties. With a higher N, we now have both hole and electron bands, and the considerations developed above now apply to both kinds of carriers (Fig. 4.2). Increasing the value of U makes the hole Fermi line smoother and tends to reduce the flap size (as has been done, e.g., in Fig. 4.2 with respect to Fig. 4.1). However, as long as the Fermi line appreciably deviates from a circle, the mean free path curve, even if it is devoid of flaps [as that of electrons in Fig. 4.2(c)], also departs from a circle and leads to a substantial modification of R_H, as well as to magnetoresistance.

For such a simple system, does a conventional two-band model provide reliable density values? In order to answer this question, we plot the real electron and hole densities as a function of N (Fig. 5), as well as the apparent values $n_{\text{app}} = p_{\text{app}}$, which would be extracted by using a procedure such as that described in Appendix B. Figure 5 indicates that n_{app} always stays around 10^{28} m^{-3}, whereas both the real electron and hole densities considerably depart from that range. Here, R_H is quite small and, depending on N, can be either positive or negative. This example also shows that, in spite of considerable variations of the real densities, n_{app} can remain remarkably stable, even if both the sign and magnitude of R_H vary.

Another lesson can be taken from Fig. 5, which can explain a relative insensitivity of the apparent densities to the electron band filling. A small value of R_H can indeed be due to several reasons. It may be induced by a compensation between holes and electrons [which cancels the numerator of R_H as given by Eq. (6)], or to a large number of just one kind of carriers (which acts on both the denominator and numerator), but it is only in the isotropic case that the common observation of a small value of R_H and of magnetoresistance indicate the presence of two kinds of carriers. Additionally, it is a common misconception to believe that Fermi lines of different perimeters (and thus of different densities) necessarily give rise to widely different σ_{XY} values, everything otherwise fixed. What matters is the variation of the mean free path along the Fermi line, as indicated by Eq. (7). If the velocities and the scattering times exhibit similar values for both the hole and electron bands,

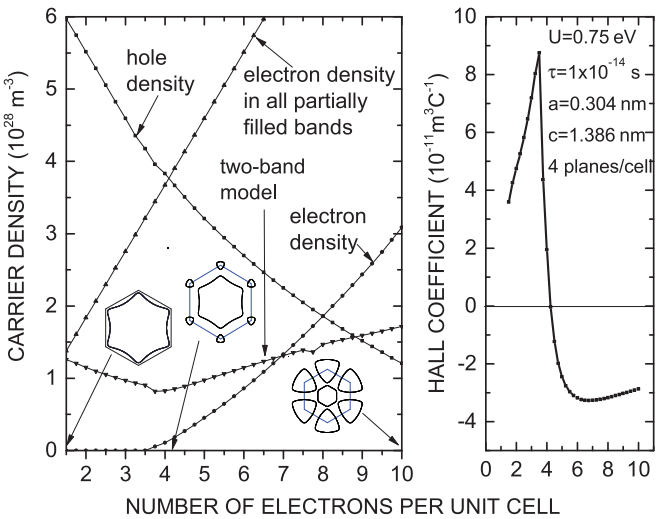

FIG. 5. (Color online) Variation of carrier densities in the various bands as a function of the number of electrons per unit cell N (left) and Hall coefficient versus N (right); hexagonal 2D NFE model. The line entitled "electron density in all partially filled bands" includes the total electron densities in both the hole and electron bands.

then the mean free paths plots will also be similar, and the number of carriers in each band is not necessarily the relevant property: both bands will give the same absolute contribution to σ_{XY}, but with opposite signs, leading to compensation and a very small R_H. In our model, similar velocities are precisely expected because both bands are derived from the very same free electron curve [see Fig. 4.2(b)]. Increasing N in Fig. 5, the electron pockets start to get filled above some threshold (and the hole concentration p decreases). After a steep variation of R_H on a narrow interval at the onset of electron filling, the pockets expand, and one rapidly reaches a kind of plateau with a negative value (Fig. 5). This plateau is a direct consequence of the considerations developed above. The degeneracy of the hole band is 1 and that of the electron pockets is 2. The mean free path curves of the hole band and one of the two electron pockets almost cancel one another out [Fig. 4.2(c)], and the net contribution to σ_{XY} is due to the second electron pocket. Since the velocity does not appreciably vary with the filling, R_H exhibits a plateau, whose value is fixed by the uncompensated electron pocket, yet p substantially decreases, whereas n increases.

D. Predicted results for MAX phases

We simply use the lattice parameters of the MAX phases and select a set of energy parameters aimed at recovering the Fermi surface of a given phase. Here, we shall focus on the case of Ti_2AlC, but we draw conclusions which can be extended to other MAX phases. Figure 6 gives the results obtained for a Fermi line mimicking the full Fermi surface of Ti_2AlC (Fig. 3, valley degeneracy $g_n = 1$ for the electron band and $g_p = 2$ for each hole band). The curves are obtained for equal electron and hole relaxation times $\tau_n = \tau_p = 10^{-14}$ s, which represent a common order of magnitude for metals [3]. Figure 6 indicates that, in spite of a minor electron contribution to ρ_{ab} (as postulated in [16]), there is a substantial contribution of all carriers to R_H. Holes alone would lead to a value of R_H almost twice higher than the expected one for the case $g_n = 1$ and $g_p = 2$ (see Fig. 6; for $g_n = g_p = 2$, the

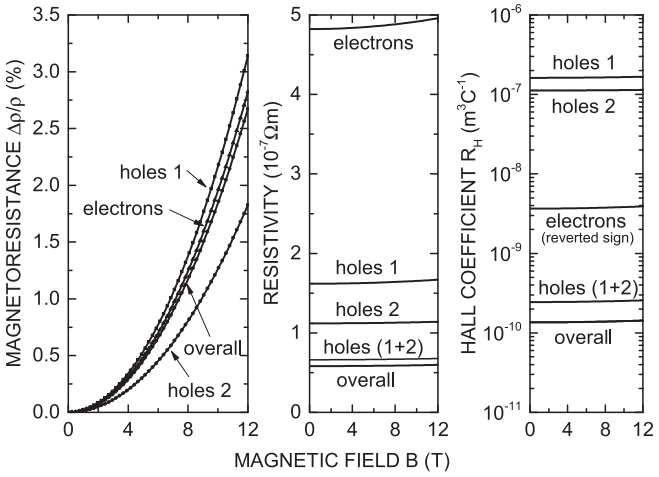

FIG. 6. Transport parameters corresponding to the 2D Fermi line mimicking the projection of the Fermi surface of Ti_2AlC (see Fig. 4) as a function of magnetic field. From left to right: magnetoresistance, resistivity, and Hall coefficient ($g_n = 1$).

difference is still larger). Any band, considered alone, exhibits a substantial magnetoresistance (see the left graph of Fig. 6), but the measured magnetoresistance is due to holes, since they give the major contribution to the overall resistivity.

A two-band isotropic model (here applied to the case $g_p = 2$ and $g_n = 1$) would give $n_{\text{app}} = p_{\text{app}} = 3.94 \times 10^{27}\ \text{m}^{-3}$, and mobilities $\mu_p \cong 148\ \text{cm}^2/\text{V.s}$ and $\mu_n \cong 125\ \text{cm}^2/\text{V.s}$, respectively (polycrystals give values around $10^{27}\ \text{m}^{-3}$ [6]). A one-band model would give only holes with $p_{\text{app}} = 4.60 \times 10^{28}\ \text{m}^{-3}$. Here, the true values are $p = 2.02 \times 10^{28}\ \text{m}^{-3}$ and $n = 2.07 \times 10^{27}\ \text{m}^{-3}$ (we note that, for a more realistic band structure, the real densities would probably be different, but would nevertheless depart from the apparent ones for the very same reasons). From this example, it is quite obvious that neither a conventional two-band model, nor a one-band model can give reasonable estimates of the true densities. The small value of R_H and the apparent compensation must not be attributed to the fact that the hole and electron densities compensate one another, since they are quite different. Firstly, we note that the velocities remain of the same order of magnitude in most parts and in any band (close to the free electron velocities). Secondly, with phonon scattering, we can reasonably expect an almost isotropic scattering time. If τ_n and τ_p are similar, the mean free path curves of any hole and electron bands are thus more or less similar. In the case of impurity scattering, we also expect similar mean free path values. Therefore, we can reasonably expect that all bands give roughly similar values of σ_{XY}. The two electron pockets per unit cell roughly compensate two hole bands. The two remaining hole bands ($g_p = 2$) give the net contribution to σ_{XY}, and since the hole density is high, R_H is small. Additionally, R_H is not only fixed by the hole density, but also by the local curvature of the Fermi line. If the hole and electron bands were in equal numbers ($g_n = g_p = 2$), we would expect an even larger compensation, not resulting from similar electron and hole concentrations. Also, in this example, the magnetoresistance is entirely due to the shape of the hole Fermi line and is not a signature of compensated transport.

Some substantial modifications are expected if τ_n and τ_p become different. Figure 7 shows the variation of the apparent two-band model density as a function of the ratio τ_n/τ_p (two cases are shown, $g_n = g_p = 2$ or $g_n = 1$ and $g_p = 2$). In practice, this ratio can differ from unity because, e.g., acoustical phonon scattering depends on the number of available final states after a collision, and the lengths of the Fermi lines of holes and electrons are different (from Fermi's golden rule, the scattering rate of a 2D isotropic band would be roughly proportional to the length of the Fermi line). Impurity scattering may also differ for electrons and holes. Figure 7 shows that a moderate change in τ_n/τ_p can produce a noticeable change in the extracted density and even reverse the sign of R_H. This sensitivity to moderate changes of some physical parameters is expected to affect the experimental data significantly. For instance, a variation of τ_n/τ_p with T might induce an apparent density variation. To confirm this, we incorporate a temperature dependence by combining the impurity and phonon scattering times τ_{imp} and τ_{ph} according to Matthiessen's rule $1/\tau = 1/\tau_{\text{imp}} + 1/\tau_{ph}$. We take $1/\tau_{ph}$ proportional to T and maintain constant the mean free path for impurity scattering λ_{imp}, so that $\tau_{\text{imp}} = \lambda_{\text{imp}}/v_{\mathbf{k}}$. Figure 8

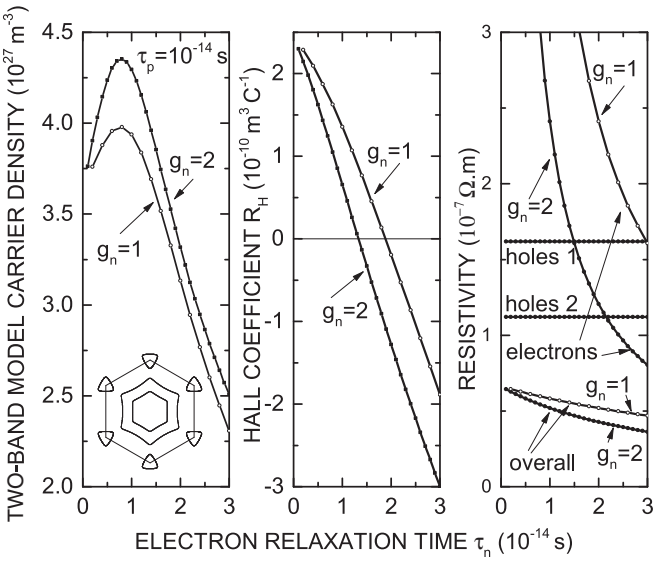

FIG. 7. For the same Fermi line as in Fig. 6, plot of the two-band model carrier density, Hall coefficient, and resistivity as a function of the electron relaxation time τ_n (τ_p being fixed).

shows the predicted temperature dependence of $n_{\rm app} = p_{\rm app}$ (conventional two-band model) and proves that a modification of τ_n/τ_p can lead to an apparent variation of the carrier density. Reasonable ratios can even lead to a substantial decrease of these densities with T, a phenomenon which cannot be explained within the frame of a physically sound isotropic model. Although not shown here, it is also not difficult to find sets of parameters for which R_H becomes almost independent of T.

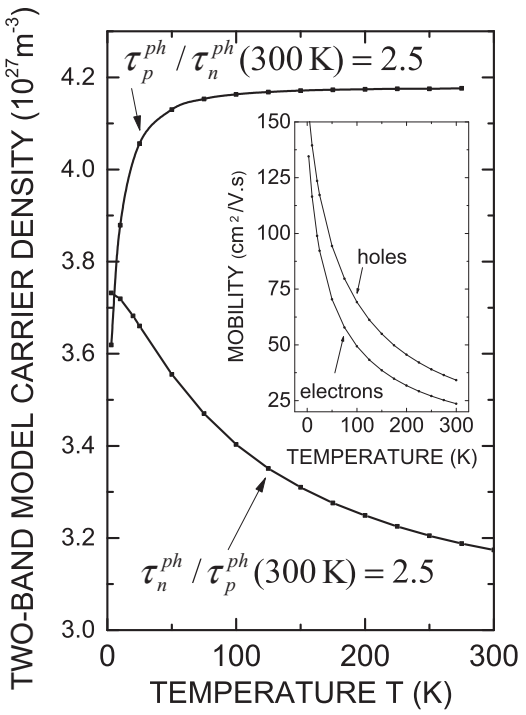

FIG. 8. For the same Fermi line as in Fig. 6, plot of the two-band model carrier density with temperature, for different room temperature ratios between the electron and hole scattering times. The insert shows the mobility.

We can now list some predictions of our 2D model, so as to compare them with the experiment reported in Sec. III. They are not only based on the data presented above, but on additional calculations carried out using, e.g., other values of U, N, band splitting, etc. First, one should observe a large anisotropy in order to justify the applicability of a 2D model to in-plane transport ($\rho_c \gg \rho_{ab}$). Secondly, for in-plane transport and assuming reasonable relaxation times for metals (from 10^{-15} to some 10^{-14} s [25]), a conventional two-band model should give extracted densities $n_{\rm app} = p_{\rm app}$ of some 10^{27} m^{-3}, and mobilities in the range of 10–500 cm^2/V.s. Here, R_H should be small, from 0 to some 10^{-10} m^{3}C^{-1}, and either negative or positive. The magnetoresistance should be of a few percent for B around 10 T.

III. EXPERIMENT

A. Sample processing and measurement principle

We can produce single crystals of Cr_2AlC, V_2AlC, Ti_3SiC_2, Nb_2AlC, and Ti_2SnC. However, the size of Nb_2AlC and Ti_2SnC crystals remains quite small (platelet area around $100 \times 100\,\mu$m), and Ti_3SiC_2 crystals are often of a lower quality and more irregular. The data reported here are thus restricted to Cr_2AlC and V_2AlC crystals of macroscopic size (less than centimeter range). Unfortunately, the calculation of the Fermi surface of those two MAX phases has not yet been achieved, so that we cannot directly use our 2D model with properly adjusted energy parameters, yet the 2D model allows us to make general predictions, and the aim of this section is to compare them with the experiment. The single-crystalline platelets were produced by high temperature solution growth (any practical detail can be retrieved from Refs. [11,12]). The crystal plane is always perpendicular to the **c** axis. The biggest crystals have areas in the range of a few centimeters squared for Cr_2AlC, and around 1 cm^2 for V_2AlC, with thicknesses t of the order of 100–200 μm for Cr_2AlC and 30–70 μm for V_2AlC. The Cr_2AlC crystals are first polished so as to obtain a uniform thickness. The as-grown V_2AlC samples do not require polishing because their thickness does not vary more than a few percent over the crystal area. Samples are patterned in two different ways: some are cut with a diamond wire saw so as to form parallelepipeds; others are defined by laser cut in order to produce Hall bars with well-defined and aligned lateral arms. Van der Pauw and Hall bar measurements are conducted from $T = 4$ to 300 K and magnetic fields B from 0 to 11 T. Injected currents are typically 10 mA. For in-plane transport measurement, the final silver paint or silver epoxy points joining the wires to the sample spread over the full edge of the samples so as to ensure a correct current injection.

All samples exhibit a small aspect ratio, which makes a correct extraction of ρ_c difficult. For such geometries, the Montgomery method [26] is not well suited, especially if the anisotropy ratio is high and varies with T [27]. The most appropriate strategy is to use conditions as close as possible to a direct measurement of ρ_c and ρ_{ab}. Here, we use a specific device structure, as proposed by Charalambous [27] and Charalambous *et al.* [28] a few decades ago for analyzing the anisotropies of the normal state resistivity of $YBa_2Cu_3O_{7-x}$. Figure 9 illustrates the device structure and

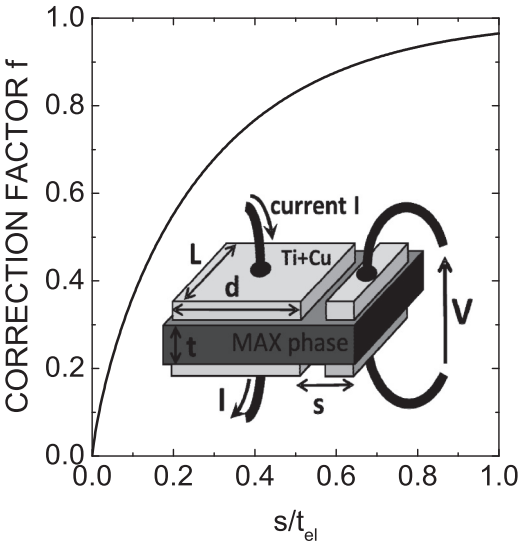

FIG. 9. Factor used for correcting the raw values of ρ_c measured using a device as described by the schematics inserted in the graph (**c** axis is perpendicular to the device plane).

measurement principle. The current is injected through large square contacts consisting of a stack of Ti or Cr (a few nanometers thick) and Cu (around 1 μm) layers. The voltage is measured through smaller lateral contacts (see Fig. 9). The raw resistance data are corrected using a factor f which is a function of sample geometry. Here, f is computed by conformal mapping of the sample [27] and is plotted in Fig. 9 as a function of the relevant geometrical factor s/t_{el}, where s is the extent of the lateral contacts and spacing (see Fig. 9), and t_{el} is the electric thickness $t_{el} = t(\rho_c/\rho_{ab})^{1/2}$ (we note that, for practical purposes, and since Ref. [27] is not available, we found that f can be approximated as $\ln(f) \cong -0.03791 + [0.7486 - 0.6617 \times (s/t_{el})^{0.307}] \times \ln(s/t_{el})$; the relative error between this formula and the original integral form is kept below a few 10^{-3} for s/t_{el} ranging from 0.03 to 1). The resistivity is calculated from [27]

$$\rho_c^{\text{corrected}} = R \times \frac{Ld}{t} \times \frac{1}{1-f}, \tag{8}$$

where R is the measured resistance, and L, d, and t are dimensions defined in Fig. 9 (for t tending to infinity, f vanishes, and the resistivity is given by the raw value RLd/t). Once ρ_c is measured, the resistivity anisotropy ratio ρ_{ab}/ρ_c is obtained by using the in-plane transport resistivity measured from a Van der Pauw sample or a Hall bar processed from a crystal issued from the same process run.

B. Anisotropy ratio ρ_c/ρ_{ab}

Figure 10 summarizes results obtained in the case of Cr_2AlC. The left graph of Fig. 10 shows the temperature variation of the raw data of ρ_c. As expected, those values vary a lot for different aspect ratios. This illustrates the incapacity of the raw data to provide reliable values. The middle graph of Fig. 10 shows the variation of the corrected ρ_c values versus T. Although the correction does not merge all curves, the maximum difference between the three samples does not

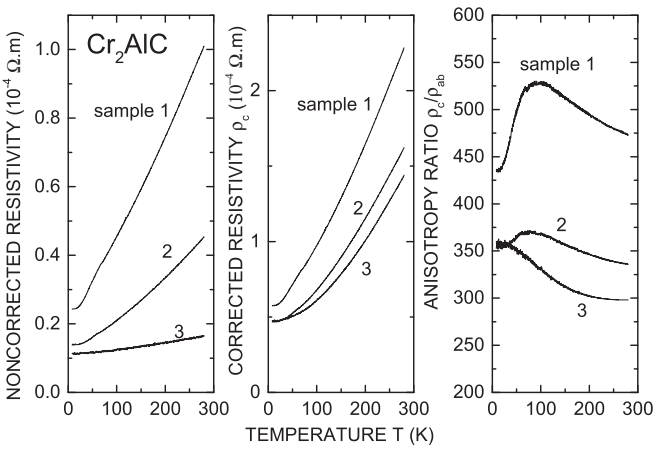

FIG. 10. Raw resistivity value, corrected resistivity value, and anisotropy ratio of three Cr_2AlC single crystals of different sizes and aspect ratios.

exceed a factor of 1.5. We attribute the residual variation to the fact that our crystals are all but perfect: Typically, the full width at half maximum of the pole figure diffraction peaks varies from 0.06 to 0.2°, so that some variability between samples and thus different relaxation times are to be expected. The anisotropy ratio is plotted in the right graph of Fig. 10. It is very substantial, in the range of a few hundreds. As in the case of $YBa_2Cu_3O_{7-x}$, ρ_c and ρ_{ab} do not exhibit the same temperature coefficient [28], so that the anisotropy ratio increases as T decreases as long as phonon scattering prevails. Plotting the same data for a V_2AlC sample shows that the anisotropy ratio is still higher, starting from 9000 at low T and decreasing down to 3000 at room temperature (Fig. 11). The anisotropies obtained for Cr_2AlC and V_2AlC are a spectacular illustration of the impact of the nanolamellar structure of the MAX phases on electrical transport and strongly support our

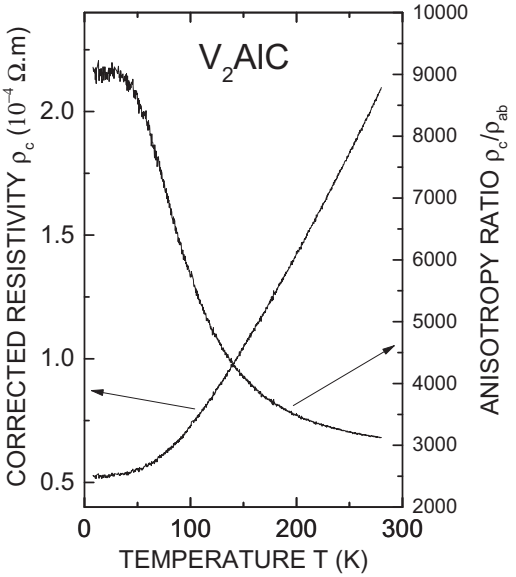

FIG. 11. Raw resistivity value, corrected resistivity value, and anisotropy ratio of a V_2AlC single crystal.

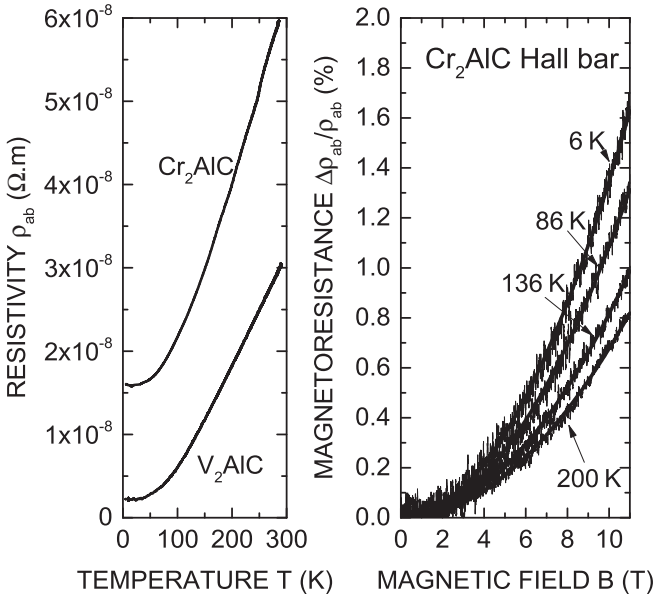

FIG. 12. Resistivity versus temperature and magnetoresistance versus magnetic field of a Hall bar (the parabolic fits cannot be distinguished from the experimental data); Cr_2AlC single crystals.

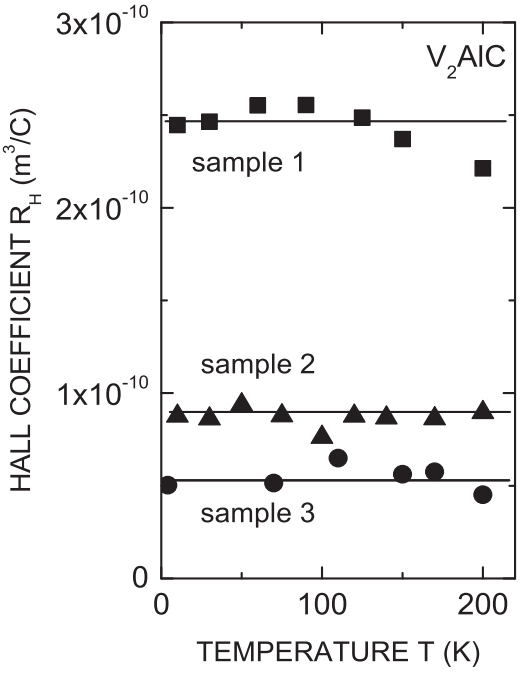

FIG. 13. Hall coefficient of three different V_2AlC single-crystalline Hall bars.

assumption of a strong spatial confinement in the transition metal planes.

C. Basal plane transport

Figure 12 (left) shows the variation of ρ_{ab} as a function of T for both Cr_2AlC and V_2AlC. The evolution is qualitatively similar to that already reported for polycrystalline phases, but the resistivity values are much lower in the case of the single crystals. The factor of improvement with respect to polycrystalline phase data [6] is around 18 for V_2AlC, and 9 for Cr_2AlC. The ratio between the room temperature value and the defect-limited value indicated by the low T plateau is equal to 14 for V_2AlC and 4 for Cr_2AlC. Since the structural quality of our crystals is not excellent [11,12], it is highly probable that these values do not represent a lower intrinsic limit, and further improvement of the materials quality should result in an additional resistivity drop. As for the polycrystalline phases, we observe a magnetoresistance of a few percent in both cases, higher for V_2AlC than for Cr_2AlC, in line with the resistivity values. This magnetoresistance decreases with T (Fig. 12), a fact that can easily be accounted for by the expected decrease of τ_n and τ_p with T. Here, R_H is small, as previously noticed for polycrystalline samples, with some variability from sample to sample (see Fig. 13 for V_2AlC and Fig. 14 for Cr_2AlC). The sign of R_H is always positive. For Cr_2AlC, this is in qualitative agreement with the result found for the polycrystalline phases [6], but for V_2AlC, negative R_H values were reported for polycrystals [6]. It is also worth noticing that different V_2AlC samples can lead to different R_H values, but there seems to be no substantial variation of R_H with T (see Fig. 13). Here, remember that, depending on the ratio chosen for τ_n/τ_p, our model can give either positive or negative values (Fig. 7). We ascribe the variability of the samples to a change in their quality, which according to our simplified 2D model can lead to substantial variations of R_H. Due to the strong T dependence of the resistivity at intermediate and high temperature, the smallness of R_H and $\Delta\rho_{ab}/\rho_{ab}$ makes them difficult to be measured, and we notice that a very slight temperature variation during a magnetic field sweep may seriously affect the final values of $\Delta\rho_{ab}/\rho_{ab}$ or R_H (typically the fluctuations of T should be less than 1%). We suspect that some of our fluctuations, as well as those reported in the literature, might be due to this artefact.

Using Cr_2AlC temperature data devoid of noise, and for which the magnetoresistance was found to be perfectly parabolic, we have extracted the carrier densities and mobilities using the conventional two-band model. The results are

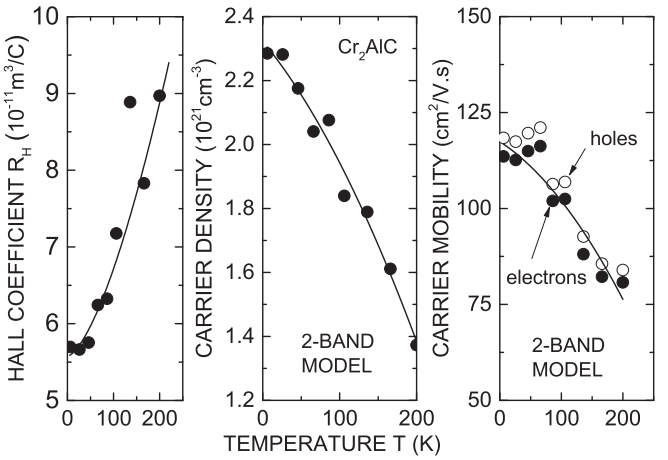

FIG. 14. Hall coefficient, two-band model density, and mobilities as a function of temperature for a Cr_2AlC Hall bar (solid lines are a guide for the eyes).

plotted in Fig. 14. The apparent carrier density $n_{app} = p_{app}$ significantly decreases with T. Such values can obviously not be equal to the real ones, which for such metallic levels and in the absence of phase transition should stay almost constant with T. This illustrates the inadequacy of the isotropic two-band model to describe MAX phases correctly, in agreement with previous observations conducted on polycrystalline Cr_2AlC [33]. Here, we note that, in spite of the frequent claim that the extracted densities are constant with T, screening the literature shows that, if this is true for a number of phases, variations may be quite substantial for many others (see, e.g., table 5.2, p. 162 in [6] and references therein). Our 2D model simply explains this apparent variation in terms of a variation in the ratio τ_n/τ_p. We find apparent densities in the range of $10^{27}\,m^{-3}$, as predicted by the 2D model (and as reported for polycrystalline phases). Apparent mobilities decrease from 120 to $70\,cm^2/V.S$ when T varies from 4 to 200 K.

IV. CONCLUSION

We have proposed a model which assumes that the carriers at the Fermi level are spatially confined in the transition metal planes, so that the MAX phases behave as quasi-2D electron systems. For some MAX phases, a NFE approach gives Fermi surfaces very close to those derived from much more elaborate techniques. The 2D model assumes a high anisotropy between ρ_{ab} and ρ_c and gives the expected orders of magnitude for the in-plane resistivity, Hall coefficient, or magnetoresistance. It is based upon the assumed shape of the Fermi line, which includes both hole bands and electron pockets. The departure of this line from a circle is responsible for an anisotropy of the in-plane velocities and for a partially compensated electron and hole behavior even when only one energy band is considered alone. It also determines the magnetoresistance. The transport properties are therefore not ultimately determined by the action of hole and electron bands, the densities of which would simply compensate one another, as in the case of an isotropic band structure, yet the small R_H values can still be partly explained by a compensation between holes and electrons. This compensation is not related to their relative densities, but to their relative velocities and mean free paths along the Fermi line. Independently of the carrier concentrations, a hole band and an electron pocket roughly give opposite contributions, as long as the velocities and scattering times on their respective Fermi lines remain similar, implying in turn similar values of the mean free path. In such a case, each electron pocket roughly compensates a hole band, and one has simply to count the number of uncompensated bands or pockets to predict the sign of R_H. However, different electron and hole scattering times can dramatically affect this prediction, as depicted in Sec. 2.4. We found that, in the case of a 2D hexagonal system of NFEs, the true electron and hole densities can vary by a considerable extent without appreciably modifying either the two-band model apparent carrier densities or the corresponding mobility values. On a numerical basis, the model might thus explain the apparent almost perfect compensation observed in the literature $n_{app} \cong p_{app}$, as well as the weak variation of n_{app} and p_{app} when passing from one phase to another.

Experimentally, we found that: (i) the anisotropy ratio of single crystals is considerable. (ii) As for polycrystalline samples, the apparent carrier densities given by a two-band model are in the range of $10^{27}\,m^{-3}$. (iii) R_H is quite small and possibly varies with T. (iv) The apparent carrier densities given by a two-band model can decrease with T (Cr_2AlC) or remain roughly constant (V_2AlC). (v) The magnetoresistance is in the range of a few percent at $B = 10\,T$. (vi) There is also a noticeable variability of the extracted parameters, which we attribute to the combination of the variability in sample quality and the sensitivity of the transport parameters on sample quality. As discussed in Sec. II, all six points above are explainable within the frame of our 2D model. Additionally, we note that points (i) and (iv) cannot be explained by a conventional one- or two-band model [unless one makes use of a pseudo-2D, isotropic model for point (i)], and that point (vi) would be difficult to explain in the case of metallic carrier densities, which are not expected to be too sensitive on defect concentration. The striking similarity between some polycrystalline and single-crystalline extracted data is yet to be explained, and no such attempt has been made in this paper.

The considerations provided in this paper and the data obtained from single crystals strongly suggest that neither a one- nor a two-band isotropic model can lead to extracted values approaching the real carrier densities and mobilities. For this reason, maybe these models should simply be dropped, or if used for the sake of comparison, it should remembered that they only deal with what the parameters of an isotropic model should be in order to exhibit equivalent transport properties. It is worth noticing that some MAX phases exhibit Fermi surfaces more complex than that given by the theory of NFEs. Some of our conclusions are therefore not necessarily applicable to these phases on a quantitative basis. Additionally, we neglected the possibility of magnetic breakdown, a phenomenon likely to happen at high field with close electron and hole Fermi surfaces. However, from the general arguments developed in this paper, it would be quite surprising that parameters extracted from isotropic models be more relevant for such complex Fermi surfaces, for which the local curvature and the velocities at the Fermi surface are the key parameters controlling transport. The Fermi surface of MAX phases has never been experimentally probed to our knowledge, yet only the experimental verification of its shape for various MAX phases can ultimately prove or invalidate our analysis.

ACKNOWLEDGMENTS

L. Shi acknowledges financial support from the "boursier FRIA", and B. Hackens is a Fonds de la Recherche Scientifique, previously Fonds National de la Recherche Scientifique (FRS-FNRS) associate researcher. This paper is financially supported by the "Agence Nationale de la Recherche" (Project ANR-13-BS09-0024).

APPENDIX A

The Ti_2AlC electronic structure calculations used to produce the Fermi surface and electron density plots of Figs. 2 and 3 were performed with the WIEN2k code [29], a DFT all electron and full potential code where Kohn-Sham orbitals are described using an augmented plane wave + local orbitals

approach. Experimental unit cell parameters from Ref. [30] were used ($\mathbf{a} = \mathbf{b} = 3.063$ Å, $\mathbf{c} = 13.680$ Å, space group: $P6_3/mmc$) and the z coordinate of the titanium atom (the only internal free parameter) was optimized. The plane wave cutoff was set to $R_{\min}K_{\max} = 7.5$ where $R_{\min}$ is the smallest muffin tin radius in the system (1.77 arb. units for the C atom in our case) and $K_{\max}$ the plane-wave momentum cutoff. The self-consistent field calculation of the potentials was performed considering 66 k-points in the irreducible part of the first Brillouin zone, and the Fermi surface calculation was performed on a denser grid of 1920 k-points. The Fermi surface and electron density plots were done using the XCrySDen software [31]. Exchange and correlation effects were treated in the generalized gradient approximation (GGA) of Perdew, Burke, and Ernzerhof [32]. Although the optimized z_{Ti} position is sensitive to the treatment of exchange and correlation effects ($z^{Ti}_{GGA} = 0.0839$ and $z^{Ti}_{LDA} = 0.0825$), we checked that the FS computed in the GGA or local density approximation (LDA) were identical.

APPENDIX B

A two-band model where electrons and holes can be described by an isotropic effective mass gives a resistivity ρ and Hall coefficient R_H of the form [3]

$$\begin{aligned}\rho &= \frac{\rho_n\rho_p(\rho_n+\rho_p)+\left(\rho_n R_p^2+\rho_p R_n^2\right)B^2}{(\rho_n+\rho_p)^2+(R_n+R_p)^2B^2},\\ R_H &= \frac{R_n\rho_p^2+R_p\rho_n^2+R_nR_p(R_n+R_p)B^2}{(\rho_n+\rho_p)^2+(R_n+R_p)^2B^2},\end{aligned} \tag{B1}$$

where the indices n and p refer to the electron and hole band, respectively, and other symbols keep their previously defined physical meaning. Assuming $n = p$ reduces those expressions and gives a resistivity $\rho = \rho_0 + \Delta\rho$ with

$$\begin{aligned}\rho_0 &= \frac{1}{ne(\mu_n+\mu_p)},\\ \frac{\Delta\rho}{\rho_0} &= \mu_n\mu_p B^2 = \alpha B^2,\end{aligned} \tag{B2}$$

and a Hall coefficient

$$R_H = \frac{R_n\left(\rho_p^2+\rho_n^2\right)}{(\rho_n+\rho_p)^2}. \tag{B3}$$

The experimental knowledge of the parabolic coefficient α of the magnetoresistance $\Delta\rho/\rho_0$, of the Hall coefficient R_H, and of the resistivity ρ_0 allows one to extract $n_{\text{app}} = p_{\text{app}}$ and the mobilities from

$$\begin{aligned}\mu_{n,p} &= \left|\frac{R_H}{2\rho_0}\left(\pm 1+\sqrt{1+4\frac{\alpha\rho_0}{R_H^2}}\right)\right|,\\ n = p &= \frac{1}{e\rho_0(\mu_n+\mu_p)}.\end{aligned} \tag{B4}$$

This is the method used to compute or extract the apparent densities and mobilities in Secs. II and III.

[1] N. P. Ong, Phys. Rev. B **43**, 193 (1991).
[2] N. C. Banik and A. W. Overhauser, Phys. Rev. B **18**, 1521 (1978).
[3] N. W. Ashcroft and N. D. Mermin, *Solid State Physics* (Saunders College, Philadelphia,1976).
[4] R. S. Allgaier, Phys. Rev. **158**, 699 (1967).
[5] U. Gottlieb, R. Laborde, and R. Madar, J. Phys. Condens. Matter **14**, 7007 (2002).
[6] M. Barsoum, *MAX phases* (Wiley, Weinheim, 2013).
[7] P. Eklund, M. Beckers, U. Jansson, H. Högberg, and L. Hultman, Thin Solid Films **518**, 1851 (2010).
[8] A. S. Farle, C. Kwakernaak, S. van der Zwaag, and W. G. Sloof, J. Eur. Ceram. Soc. **35**, 37 (2015).
[9] M. Naguib, M. Kurtoglu, V. Presser, J. Lu, J. Niu, M. Heon, L. Hultman, Y. Gogotsi, and M. W. Barsoum, Adv. Mater. **23**, 4248 (2011).
[10] A. S. Ingason, A. Mockute, M. Dahlqvist, F. Magnus, S. Olafsson, U. B. Arnalds, B. Alling, I. A. Abrikosov, B. Hjörvarsson, P. O. Persson, and J. Rosen, Phys. Rev. Lett. **110**, 195502 (2013).
[11] L. Shi, T. Ouisse, E. Sarigiannidou, O. Chaix-Pluchery, H. Roussel, D. Chaussende, and B. Hackens, Acta Mater. **83**, 304 (2015).
[12] T. Ouisse, E. Sarigiannidou, O. Chaix-Pluchery, H. Roussel, B. Doisneau, and D. Chaussende, J. Cryst. Growth **384**, 88 (2013).
[13] F. Mercier, T. Ouisse, and D. Chaussende, Phys. Rev. B **83**, 075411 (2011).
[14] J. Emmerlich, H. Högberg, S. Sasvari, P. O. A. Persson, L. Hultman, J. P. Palmquist, U. Jansson, J. M. Molina-Aldareguia, and Z. Czigany, J. Appl. Phys. **96**, 4817 (2004).
[15] M. Magnuson, M. Mattesini, N. V. Nong, P. Eklund, and L. Hultman, Phys. Rev. B **85**, 195134 (2012).
[16] V. Mauchamp, W. Yu, L. Gence, L. Piraux, T. Cabioc'h, V. Gauthier, P. Eklund, and S. Dubois, Phys. Rev. B **87**, 235105 (2013).
[17] P. Eklund, M. Bugnet, V. Mauchamp, S. Dubois, C. Tromas, J. Jensen, L. Piraux, L. Gence, M. Jaouen, and T. Cabioc'h, Phys. Rev. B **84**, 075424 (2011).
[18] P. Finkel, J. D. Hettinger, S. E. Lofland, M. W. Barsoum, and T. El-Raghy, Phys. Rev. B **65**, 035113 (2001).
[19] P. Finkel, M. W. Barsoum, J. D. Hettinger, S. E. Lofland, and H. I. Yoo, Phys. Rev B **67**, 235108 (2003).
[20] P. Finkel, B. Seaman, K. Harrel, J. Palma, J. D. Hettinger, S. Lofland, A. Ganguly, M. W. Barsoum, and Z. Sun, Phys. Rev B **70**, 085104 (2004).
[21] J. D. Hettinger, S. E. Lofland, T. Meehan, J. Palma, K. Harrel, S. Gupta, A. Ganguly, T. El-Raghy, and M. W. Barsoum, Phys. Rev B **72**, 115120 (2005).
[22] T. H. Scabarozi, S. Amini, P. Finkel, O. D. Leaffer, J. E. Spanier, M. W. Barsoum, M. Drulis, H. Drulis, W. M. Tambussi,

J. D. Hettinger, and S. E. Lofland, J. Appl. Phys. **104**, 033502 (2008).
[23] L. Chaput, G. Hug, P. Pécheur, and H. Scherrer, Phys. Rev. B **71**, 121104(R) (2005).
[24] L. Chaput, G. Hug, P. Pécheur, and H. Scherrer, Phys. Rev. B **75**, 035107 (2007).
[25] J. M. Ziman, *Electrons and Phonons* (Clarendon Press, Oxford, 1960).
[26] H. C. Montgomery, J. Appl. Phys. **42**, 2971 (1971).
[27] M. Charalambous, PhD Thesis, University of Grenoble, 1992.
[28] M. Charalambous, J. Chaussy, and P. Lejay, Phys. Rev. B **45**, 5091 (1992).
[29] P. Blaha, K. Schwarz, G. K. H. Madsen, D. Kvaniscka, and J. Luitz, *WIEN2k, An Augmented Plane Wave + Local Orbitals Program for Calculating Crystal Properties* (Technische Universität WIEN, Austria, 2001).
[30] W. Yu, V. Mauchamp, T. Cabioc'h, D. Magne, L. Gence, L. Piraux, V. Gauthier-Brunet, and S. Dubois, Acta Mater. **80**, 421 (2014).
[31] A. Kokalj, Comput. Mater. Sci. **28**, 155 (2003).
[32] J. P. Perdew, K. Burke, and M. Ernzerhof, Phys. Rev. Lett. **77**, 3865 (1996).
[33] M. W. Barsoum, T. H. Scabarozi, S. Amini, J. D. Hettinger, and S. E. Lofland, J. Am. Ceram. Soc. **94**, 4123 (2011).